Nanoscale

Accepted Manuscript

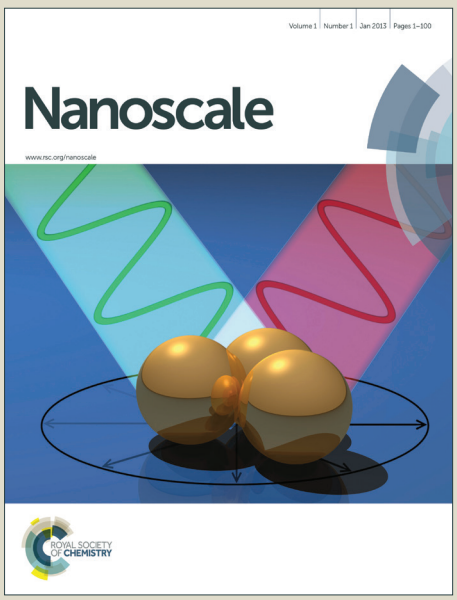

ROYAL SOCIETY OF CHEMISTRY

www.rsc.org/nanoscale

Journal Name

RSCPublishing

ARTICLE

Generic Phosphatase Activity Detection using Zinc Mediated Aggregation Modulation of Polypeptide-Modified Gold Nanoparticles

Cite this: DOI: 10.1039/x0xx00000x

Received 00th January 2012,
Accepted 00th January 2012

DOI: 10.1039/x0xx00000x

www.rsc.org/

Robert Selegård, Karin Enander, Daniel Aili*

A challenge in the design of plasmonic nanoparticle-based colorimetric assays is that the change in colloidal stability, which generates the colorimetric response, is often directly linked to the biomolecular recognition event. New assay strategies are hence required for every type of substrate and enzyme of interest. Here, a generic strategy for monitoring of phosphatase activity is presented where substrate recognition is completely decoupled from the nanoparticle stability modulation mechanism, which enables detection of a wide range of enzymes using different natural substrates with a single simple detection scheme. Phosphatase activity generates inorganic phosphate that forms an insoluble complex with Zn^{2+}. In a sample containing a preset concentration of Zn^{2+}, phosphatase activity will markedly reduce the concentration of dissolved Zn^{2+} from the original value, which in turn affects the aggregation of gold nanoparticles functionalized with a designed Zn^{2+} responsive polypeptide. The change in nanoparticle stability thus provides a rapid and sensitive readout of the phosphatase activity. The assay is not limited to a particular enzyme or enzyme substrate, which is demonstrated using three completely different phosphatases and five different substrates, and thus constitutes a highly interesting system for drug screening and diagnostics.

Introduction

The high-energy phosphate ester bonds in nucleoside 5´-triphosphates (NTPs) are the primary energy carriers in cells and are consumed and produced in a countless number of metabolic reactions as the need for energy fluctuates. NTPs are not only ubiquitous energy donors but are also involved in numerous other critically important processes. Adenosine 5´-triphosphate (ATP) is a neurotransmitter and an essential component in the purinergic signaling system which regulates cellular functions through autocrine and paracrine activation of nucleotide receptors,[1, 2] while guanosine 5´-triphosphate (GTP) is involved in G-protein mediated cellular signaling,[3] protein synthesis,[4] and vesicular transport.[5] The phosphate ester bond is also present in pyrophosphate (PP_i), which in higher organisms is generated by metabolic degradation of NTPs, and plays a critical role in regulating extracellular matrix calcification. In certain lower organisms it can act as an ATP substitute under anaerobic conditions.[6] Both intra and extracellular levels of these phosphate ester-containing compounds (from now on denoted PP_x) are regulated and hydrolyzed by a large number of phosphatases, releasing inorganic phosphates (P_i) as byproducts. The human genome is also encoding for hundreds of different protein phosphatases that hydrolyze phosphoric monoester modifications of proteins and that act in concert with kinases to regulate a plethora of critically important cellular processes such as metabolic activity,[7] cell motility,[8] cell survival and cell death.[9] Assays that can monitor phosphatase activity can thus be used to characterize a vast number of fundamentally important enzymatic reactions and potential drug targets and are regularly used for diagnosis of a range of diseases, and are consequently of immense importance for biomedical research, drug development, and diagnostics.

Conventional methods for monitoring phosphatase mediated hydrolysis of NTP and PP_i exploit synthetic substrate analogues that produce a change in color,[10] luminesce[11] or fluorescence[12] when hydrolyzed. Although sensitive, these types of assay are subjected to interference from compounds in the sample with similar optical properties. Moreover, they rely on the use of non-natural substrates that can give an erroneous interpretation of enzymatic activity.

The use of gold nanoparticles (AuNPs) as transducers in colorimetric assays has received considerable attention due to their unique optical properties, tunable surface chemistry and potentially very high sensitivity.[13-15] In particular the colorimetric response generated as a consequence of aggregation or redispersion of AuNPs has been utilized in a wide range of applications, including detection of enzymes,[16-18] nucleotides,[19] and metal cations.[20, 21] Assays for the detection of phosphatase activity have also been reported but either use non-functionalized AuNPs that are prone to unspecific aggregation

or are restricted to the use of a specific substrate.[22-24] The latter reflects a general problem in design of AuNP-based assays; that the change in colloidal stability is directly linked to the biomolecular recognition event. New assay strategies are thus required for every type of substrate and enzyme of interest, which is both time-consuming and expensive. Here, we present a generic AuNP-based strategy for monitoring of enzymatic PP_x hydrolysis where substrate recognition is completely decoupled from the nanoparticle stability modulation mechanism, which enables detection of a wide range of enzymes using different natural substrates and a single detection scheme.

PP_x and other phosphate containing species have in common that they readily coordinate metal cations such as Mg^{2+}, Mn^{2+} and Zn^{2+}.[25, 26] In fact, virtually all reactions involving NTPs also involve metal cations directly coordinated to the nucleotides or as integrated cofactors in the hydrolytic enzymes.[27] Even though the coordination capacity varies between different PP_x species, they have in common that P_i is generated when they are hydrolyzed. The coordination capacity of P_i for Zn^{2+} is higher compared to the starting materials, and the resulting complex, $[Zn_3(PO_4)_2]$, is virtually insoluble. Enzymatic hydrolysis of PP_x to P_i hence provides a mechanism to regulate the concentration of dissolved Zn^{2+} in a sample. In our approach to monitoring enzymatic PP_x hydrolysis, we exploit this mechanism to tune the colloidal stability of AuNPs functionalized with a Zn^{2+} responsive *de novo* designed polypeptide. The enzymatic generation of P_i and the subsequent formation of insoluble Zn^{2+} complexes reduces the concentration of Zn^{2+} available to the polypeptide, which has a dramatic effect on the stability of the AuNPs. Aggregation of the polypeptide-functionalized AuNPs is triggered in a rather narrow Zn^{2+} concentration interval as a consequence of a Zn^{2+}-induced folding of the immobilized polypeptides.[21] Even very subtle changes in the concentration of Zn^{2+} can result in drastic changes in the AuNP aggregation, which affects the localized surface plasmon resonance (LSPR) band, producing a colorimetric response. By maintaining a constant concentration of both Zn^{2+} and PP_x, the colloidal stability of the AuNPs and hence the color of the suspension reflects the affinity and coordination number of the compounds interacting and forming complexes with Zn^{2+}.[28]

The Zn^{2+}-triggered AuNP aggregation is highly specific and the result of a Zn^{2+}-dependent homodimerization and folding of the immobilized polypeptides (JR2EC).[21] JR2EC is a 42 residue helix-loop-helix polypeptide designed to homodimerize and fold into a molten globule-like antiparallel four-helix bundle when subjected to Zn^{2+}. The folding is primarily driven by the burial of non-polar residues resulting in a formation of a hydrophobic core. The peptide contains a large number of glutamic acid residues mainly situated at the dimerization interface. At a neutral pH these residues give the peptide a net charge of -5 and charge-repulsion between monomers effectively prevents homodimerization. The addition of Zn^{2+} decreases the charge-repulsion, and folding and the subsequent homodimerization are induced.[21] The peptides were immobilized on citrate stabilized AuNPs via a cysteine residue in the loop region, yielding particles with a remarkably high colloidal stability.[16] By exposing the polypeptide functionalized particles (JR2EC-AuNPs) to millimolar concentrations of Zn^{2+} a dramatic and immediate aggregation is induced. The aggregation is a result of the joint coordination of Zn^{2+} by peptides immobilized on separate AuNPs, resulting in a folding-dependent supramolecular nanoparticle bridging. The concomitant LSPR shift saturates in a matter of minutes and can be monitored spectroscopically by tracking the change in the position of the plasmon band maximum ($\Delta\lambda_{max}$). We have previously employed this highly controllable Zn^{2+}-induced aggregation in combination with synthetic receptors for colorimetric detection of proteins and for studies of the mechanism of Zn^{2+} coordination between proteins and biologically relevant low molecular weight chelants.[17, 28] By exploiting the enzymatic hydrolysis of PP_x to regulate the Zn^{2+} concentration and thus the stability of the AuNPs we have found an attractive route for monitoring the activity of a wide range of phosphatases and which is not restricted to the use of a specific substrate. We further envision that this novel approach to modulate nanoparticle stability can be used not only for sensing of phosphatase activity but to monitor virtually any chemical reaction that demonstrate a difference in the Zn^{2+} chelating properties of the starting materials and the resulting products. This inherent flexibility, combined with the possibilities to rapidly monitor enzymatic activity on natural substrates with high sensitivity using low-cost equipment, make this technology highly suitable for a range of applications including diagnostics and high throughput drug screening.

Results and discussion

We modified AuNPs with the zinc responsive polypeptide JR2EC to obtain a hybrid material that enabled us to monitor phosphatase-triggered changes in Zn^{2+} concentration by means of the associated effects on the colloidal stability of the nanoparticles. JR2EC was immobilized on 20 nm citrate stabilized AuNPs using the cysteine residue in the loop region. Unbound polypeptides were removed by repeated centrifugations and resuspension in Bis-tris buffer (30 mM, pH 7) until the concentration of polypeptides in solution was lower than 5 pM. Unmodified AuNPs subjected to this treatment aggregated extensively and non-reversibly whereas the peptide functionalized AuNPs displayed excellent colloidal stability as a result of efficient electrosteric stabilization by the highly negatively charged JR2EC. JR2EC-AuNPs aggregated rapidly but reversibly when exposed to Zn^{2+} concentrations > 1 mM, causing a red shift of the LSPR band from ~527 nm to ~610 nm (Figure 1a), resulting in a clearly visible color change of the suspension. The particles went from a completely dispersed state to a state of extensive aggregation in a narrow Zn^{2+} concentration range, 1-1.5 mM (Figure 1b).[21, 28] Addition of Zn^{2+} coordinating compounds can reduce the concentration of Zn^{2+} available to the peptide, which consequently affect the aggregation. One such compound capable of sequestering Zn^{2+} is inorganic phosphate (P_i), which forms insoluble $[Zn_3(PO_4)_2]$

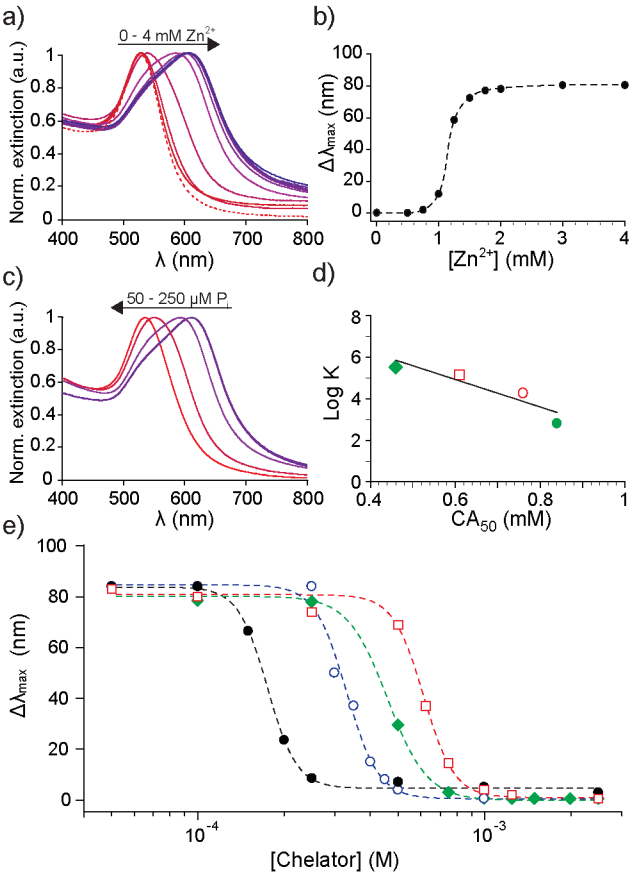

Figure 1 a) UV-vis spectra of JR2EC-AuNPs in the presence of increasing concentrations of Zn^{2+}, from 0 mM (broken line) to 4 mM. b) Change in the position of the LSPR peak maximum ($\Delta\lambda_{max}$) as a function of increasing Zn^{2+} concentration, from 0 mM to 4 mM. c) UV-vis spectra of JR2EC-AuNPs upon addition of P_i (50 - 250 µM) in the presence of 2 mM Zn^{2+}. d) Linear correlation between log K and CA_{50} for GTP (♦), ATP (□), ADP (○) and GMP (●) which all interact in a 1:1 stoichiometry with Zn^{2+}. e) $\Delta\lambda_{max}$ as a function of [P_i] (●), [PP_i] (○), [GTP] (♦) and [ATP] (□) in a buffer containing 2 mM Zn^{2+}. Lines in b) and e) were obtained by fitting data to a monophasic Hill equation.

complexes with a logarithmic solubility product constant (log K_{sp}) of -31.49.[29] Sufficiently high concentrations of P_i can efficiently deprive the immobilized polypeptides of Zn^{2+}, preventing aggregation.

When keeping the concentration of Zn^{2+} constant at 2 mM, which in the absence of competing chelators is high enough to cause massive aggregation, a gradual decrease in aggregation was observed with increasing concentration of P_i from 100 µM to 250 µM (Figure 1c and e). At 250 µM P_i the particles were completely dispersed. Considering the stoichiometry of forming $Zn_3(PO_4)_2$, this amount of P_i will reduce the Zn^{2+} concentration in solution to about 1.63 mM, which in the absence of P_i is still enough to induce extensive aggregation (Figure 2b). The prevention of the normal mode of aggregation did thus occur at a lower concentration of P_i than to be expected by the decrease in the Zn^{2+} concentration alone (Figure S1). We have recently shown that chelants with a coordination number of >1 and capable of forming ternary complexes with Zn^{2+} can share the metal ion with the peptide. These interactions result in formation of a network polynuclear complexes that are tethered to the nanoparticle surface via the peptide-associated Zn^{2+} and which consequently interferes with peptide dimerization and prevents the folding induced aggregation.[28] In addition to the decrease in the concentration of available Zn^{2+}, the aggregation is thus likely affected by the formation of ternary complexes involving JR2EC as a ligand that share the Zn^{2+} with P_i in order to create a full coordination sphere. The polypeptide-Zn^{2+}-P_i complex can then anchor $[Zn_3(PO_4)_2]$ complexes to the nanoparticle surface.

A similar effect was observed for PP_i but the concentration required to completely prevent aggregation was significantly higher. This difference can be illustrated by comparing the concentration of coordination agent required to reduce the maximum LSPR response by 50% (CA_{50}), which was 0.17 mM and 0.33 mM for P_i and PP_i respectively. These values were obtained by fitting the data in Figure 1e) to a monophasic Hill equation (Supporting Information). PP_i forms complexes with Zn^{2+} predominantly in the soluble form of $[Zn^{2+}(PP_i)_2]^{6-}$ with a logarithmic stability constant (log K) of 11.0.[25] The lower Zn^{2+} affinity and stoichiometry explains the lower CA_{50} value obtained for PP_i as compared to P_i. The presence of both P_i and PP_i could thus easily be detected and discriminated using this plasmonic assay because the latter was required in significantly higher concentrations to prevent nanoparticle aggregation (Figure 1 e).

This is particularly interesting since both species are generated as byproducts in numerous critically important enzymatic reactions. For example, P_i can be generated by hydrolysis of NTPs such as ATP and GTP. Both ATP and GTP, as well as nucleotide mono- and di-phosphates, form monomeric complexes with divalent metal ions, albeit with lower affinity than P_i and PP_i. The stability and solubility constants for the complex formation between Zn^{2+}, Mg^{2+}, Ca^{2+} and these species are summarized in Table 1. The coordination of Zn^{2+} by ATP and GTP was clearly visualized using the polypeptide functionalized AuNPs (Figure 1e). GTP, which has slightly higher affinity for Zn^{2+} than ATP, was indeed found to prevent the Zn^{2+} triggered aggregation to a larger extent than ATP, with a CA_{50} of 0.46 mM and 0.61 mM for GTP and ATP, respectively (Figure 1e).[26] The same trend was observed for adenosine 5'-diphosphate (ADP), guanosine 5'-monophosphate (GMP), adenosine 5'-monophosphate (AMP), and adenosine, where higher concentrations were required to prevent aggregation as the affinity for Zn^{2+} decreased (Table 1 and Figure S2).[30, 31] AMP was however insoluble at the concentrations required to completely prevent aggregation, but initially showed the same trend. The nucleoside adenosine had a negligible influence on the stability of the JR2EC-AuNPs, since the affinity was too low to deprive the polypeptide of enough Zn^{2+} to affect the aggregation. A linear correlation was found between the log K value and CA_{50} for the species that formed monomeric complexes with Zn^{2+} (GTP, ATP, ADP and GMP) and that could prevent the aggregation (Figure 1d), demonstrating the clear correlation between the solubility constant and the CA_{50} value.

Table 1. Stability and solubility constants and CA_{50} values for complexes

	log K [a]			log K_{sp} [b]			Ref.	CA_{50} [mM] [c]
	Zn^{2+}	Mg^{2+}	Ca^{2+}	Zn^{2+}	Mg^{2+}	Ca^{2+}		
ATP	5.16	4.29	3.91	-	-	-	26	0.61
ADP	4.28	3.36	2.95	-	-	-	30	0.76
AMP	2.38	1.62	1.48	-	-	-	30	-
Adenosine	0.24	-	-	-	-	-	30	-
GTP	5.52	4.31	3.96	-	-	-	26	0.46
GMP	2.65	1.54	1.73	-	-	-	31	0.84
P_i	-	-	-	-31.49	-25	-32.68	29	0.17
PP_i	11.0	-	-	-	-	-	25	0.33

[a] Logarithmic stability constant of complexes with Zn^{2+}, Ca^{2+} and Mg^{2+}. [b] Logarithmic solubility constant for $Zn_3(PO_4)_2$ in water. [c] Concentration required to reduce the maximum Zn^{2+}-response by 50%.

It should be mentioned that the Bis-Tris buffer used here also can coordinate Zn^{2+} to a certain extent and has been found to stabilize ATP-Zn^{2+} complexes as an additional ligand.[26] This effect will however not influence the ability of the system to detect changes in the total Zn^{2+} coordination capacity of the sample as a result of enzymatic hydrolysis of NTP.

Plasmonic detection of phosphatase activity

PP_x are common substrates in numerous enzyme-regulated reactions where the high-energy ester bonds are hydrolyzed to yield 2-3 P_i for each substrate. The number of P_i generated is dependent on the substrate and the particular enzyme involved. We investigated three different enzymes; alkaline phosphatase (ALP), pyrophosphatase (PPase) and apyrase, using five different substrates (ATP, ADP, AMP, GTP, and PP_i) in order to validate the hypothesis that the proposed system can be utilized as a generic sensing strategy for monitoring enzymatic processes generating P_i (Figure 2a).

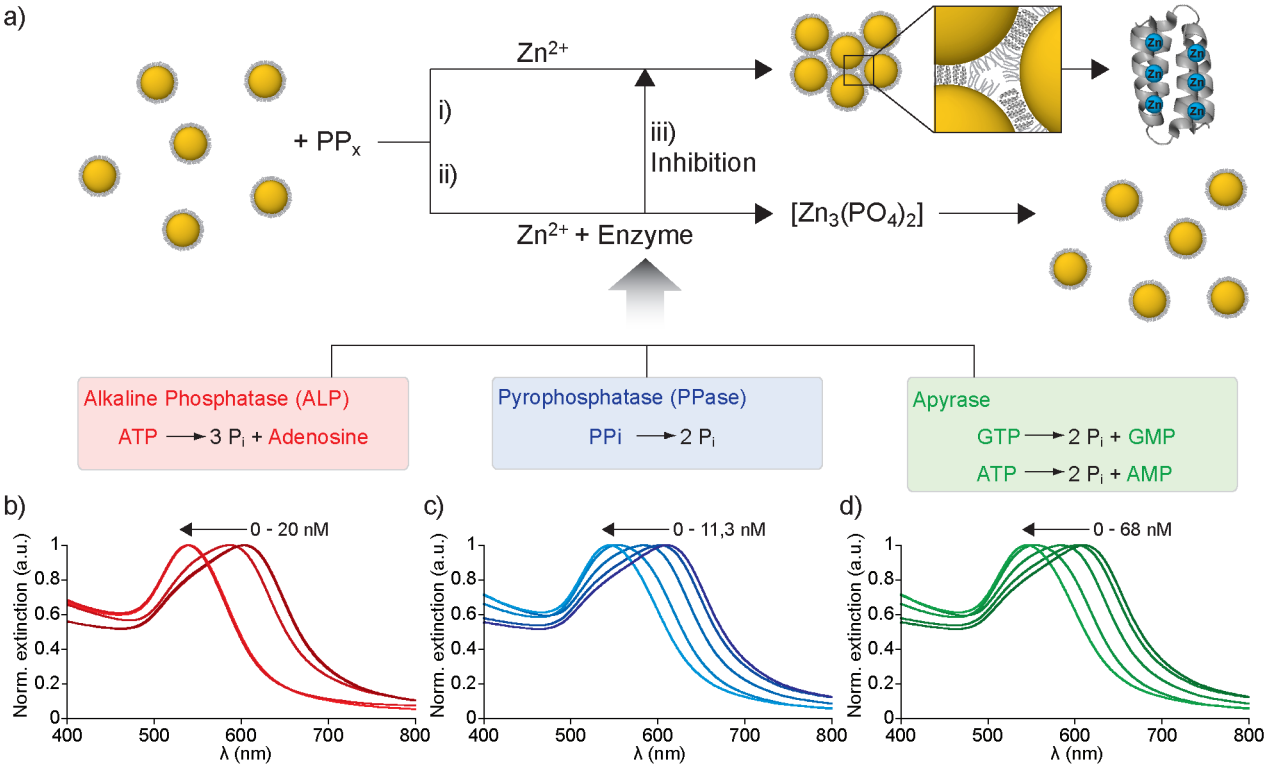

Figure 2 a) Schematic illustration of the generic phosphatase assay: i) Low concentrations of PP_x cannot coordinate enough Zn^{2+} to prevent the Zn^{2+}-dependent folding-induced aggregation of JR2EC-AuNPs. ii) Enzymatic hydrolysis of ATP by ALP, PP_i by PPase or GTP/ATP by apyrase generates P_i which forms insoluble complexes with Zn^{2+}. The reduced Zn^{2+} concentration prevents nanoparticle aggregation. iii) Inhibition of phosphatase activity results in a dose dependent effect on the aggregation enabling inhibitor characterization. b)-d) Concentration dependent shift of the LSPR band of JR2EC-AuNPs in 2 mM Zn^{2+} as a result of b) ALP (0-20 nM) hydrolyzation of ATP (100 µM) at 37°C for 1 hour c) PPase (0-11.3 nM) hydrolyzation of PP_i (175 µM) at 30°C for 10 min d) apyrase (0-68 nM) hydrolyzation of GTP (250 µM) at 30°C for 2.5 hours.

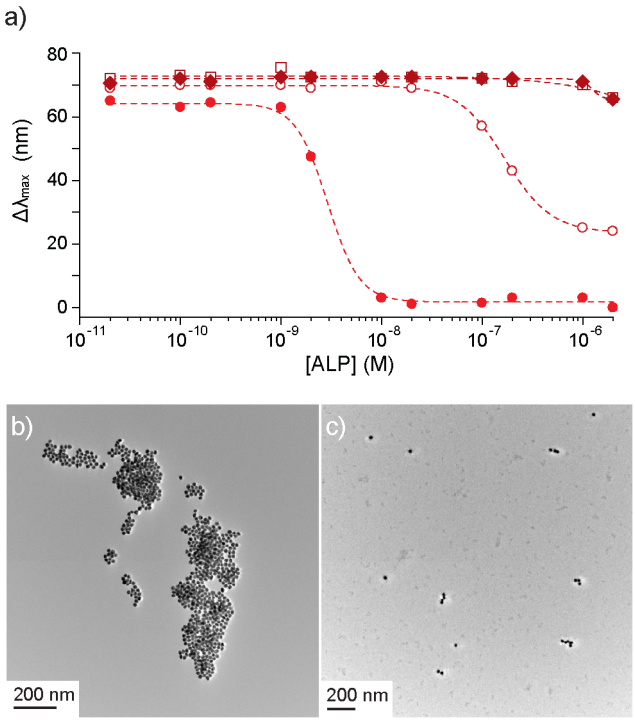

Figure 3 a) ALP concentration dependent LSPR peak shifts of JR2EC-AuNPs in 2 mM Zn^{2+} and 100 µM ATP (●), ADP (○), AMP (♦) or adenosine (□). b) and c) Transmission electron micrographs of JR2EC-AuNPs in the presence of (b) 2 mM Zn^{2+} and 100 µM ATP and (c) 20 nM ALP pre-incubated with 100 µM ATP for 30 min at 37 °C prior to addition of 2 mM Zn^{2+} and JR2EC-AuNPs.

ALP catalyzes the dephosphorylation of ATP yielding a maximum of 3 P_i per ATP (Figure 2a). The ALP activity was monitored by incubating ATP (100 µM) with ALP (0-20 nM) in a Tris buffer (50 mM, pH 9) containing 1 mM Mg^{2+} for 1 hour at 37 °C prior to addition to a buffer containing 2 mM Zn^{2+} and JR2EC-AuNPs (70 pM). The shift in the LSPR band was approximately 65 nm from lowest to highest concentration of ALP yielding almost completely dispersed particles at 10 nM ALP (Figure 2b). No effect on the aggregation was observed in the absence of ALP (100 µM ATP and 2 mM Zn^{2+}) or in the absence of ATP (2 µM ALP and 2 mM Zn^{2+}) (Figure S3), which clearly demonstrates that the combination of both ALP and ATP was required to prevent the Zn^{2+}-triggered nanoparticle aggregation and that the effect was indeed specific. ALP activity required addition of the cofactor Mg^{2+} (50 µM). The stability constants of complexes between Mg^{2+} and ATP, ADP and AMP are about one order of magnitude lower than the corresponding interactions with Zn^{2+}(Table 1) and will thus not significantly affect the formation of Zn^{2+} complexes.[26, 30] Mg^{2+} can also form complexes with P_i but these are about 6 orders of magnitude more soluble than the corresponding Zn^{2+} complex.[29] Moreover, Mg^{2+} does not induce folding of JR2EC and the addition the Mg^{2+} concentrations required for ALP activity did hence not influence the detection mechanism ensuring that Zn^{2+} was the main stability modulator.[21,]

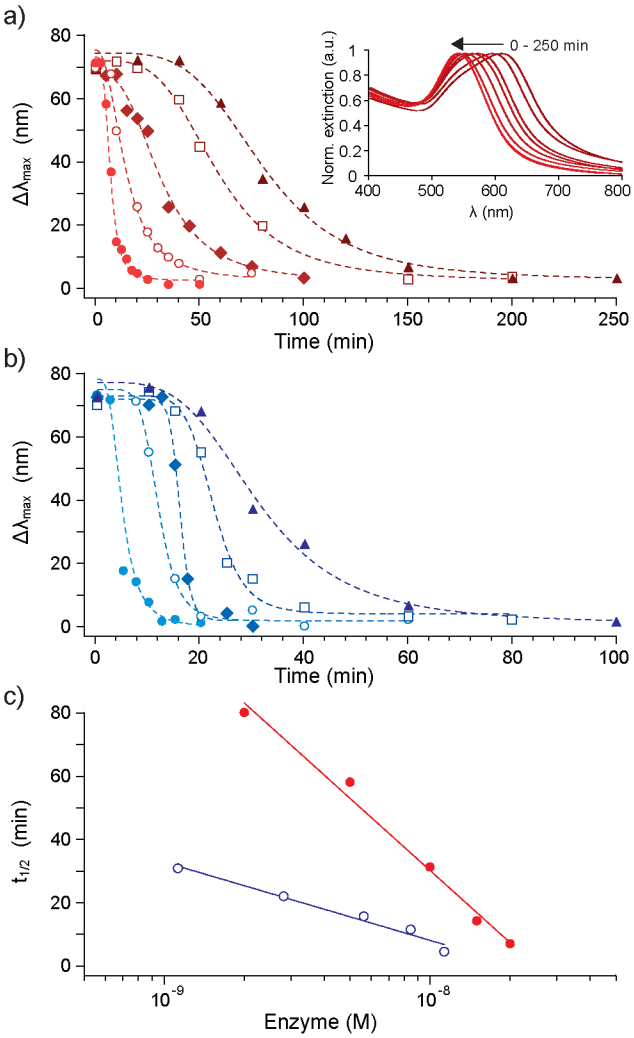

Figure 4 a) Time dependent LSPR peak shifts of JR2EC-AuNPs after exposure to 2 mM Zn^{2+}, 100 µM ATP and 2 (▲), 5 (□), 10 (♦), 15 (○) and 20 nM (●) ALP. Inset: Time dependent shift (0-250 min) of the LSPR band of JR2EC-AuNPs in 2 mM Zn^{2+} as a result of 2 nM ALP hydrolyzation of ATP (100 µM at t= 0 min) at 37 °C. b) Time dependent LSPR peak shifts of JR2EC-AuNPs as a result of exposure to 2 mM Zn^{2+} and samples containing 175 µM PP_i and 1.1 (▲), 2.8 (□), 5.6 (♦), 8.5 (○) and 11.3 nM (●) PPase. Lines in a) and b) were obtained by fitting data to a monophasic Hill equation. c) Time required for obtaining 50% LSPR response as a function of enzyme concentration for ALP (●, red, R^2 = 0.98) and PPase (○, blue, R^2 = 0.97) obtained from the fitted data in a) and b).

Substituting ATP for ADP as the ALP substrate under otherwise identical conditions required a higher concentration of ALP to generate enough P_i to prevent nanoparticle aggregation (Figure 3a). Because the enzymatic degradation of 100 µM ADP can accumulate a maximum of 200 µM P_i, the dispersion of the JR2EC-AuNPs was not complete since complete dispersion would require at least 250 µM P_i (Figure 1e). A $\Delta\lambda_{max}$ of approximately 20 nm was consequently obtained which is in excellent agreement with the $\Delta\lambda_{max}$ obtained for 200 µM P_i (Figure 1e), indicating that the added ADP was completely hydrolyzed within 1 hour.

When substituting ADP for AMP not enough P_i was generated to prevent aggregation independently of the concentration of ALP because a maximum of 100 µM P_i will result from a complete hydrolysis of AMP. Consequently,

substituting AMP for adenosine had no impact on the modulation as no P_i could be liberated. This set of experiments clearly demonstrates that the assay can be used to detect and discriminate ALP activity on all of the different natural substrates: adenosine mono-, di- and tri-phosphates, by simply utilizing an appropriate initial substrate concentration.

Transmission electron micrographs of JR2EC-AuNPs exposed to 2 mM Zn^{2+} and 100 µM ATP, with and without the preceding enzymatic hydrolysis with 20 nM ALP for 30 min at 37 °C, further confirmed the spectroscopic observations (Figure 3 b-c). In samples not treated with ALP large JR2EC-AuNP aggregates were dominant whereas in samples treated with ALP only small aggregates and dispersed particles were present. In the former sample the corresponding Δλmax value was about 65 nm whereas no shift in the LSPR band was seen in the absence of ALP. In figure 3 c) small precipitates presumably comprised of $[Zn_3(PO_4)_2]$ are clearly seen in addition to the particles.

The ALP concentration dependent generation of P_i was further characterized as a function of time. ALP (2-20 nM) was pre-incubated with ATP (100 µM) for various times at 37 °C. The time required for ALP to generate enough P_i to prevent nanoparticle aggregation was highly dependent on the ALP concentration (Figure 4a). The time required for obtaining a 50 % LSPR response ($t_{½}$) was found to be linearly dependent of log[ALP] (Figure 4c), where the slope of the curve is directly proportional to the catalytic activity of the enzyme for the selected substrate.

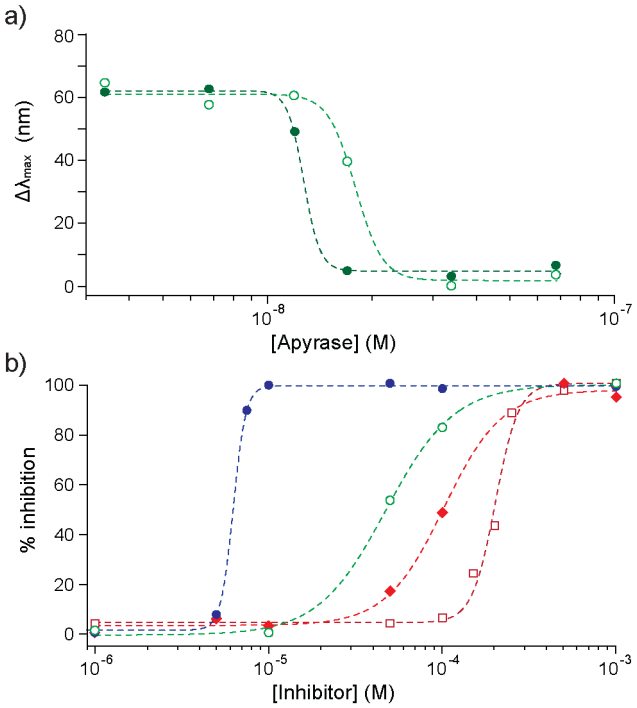

Figure 5 a) Change in LSPR peak position of JR2EC-AuNPs as a result of exposure to 2 mM Zn^{2+} and samples containing 250 µM ATP (●) and GTP (○) incubated with 3.4–68 nM apyrase for 2.5 hours at 30 °C. b) Inhibition of the three phosphatases as a function of concentration inhibitor. ALP (20 nM) was incubated with 10^{-6}-10^{-3} M theophylline (♦) or Na_3VO_4 (□) and 100 µM ATP for 30 min at 37 °C in a buffer containing 1 mM Mg^{2+}. PPase (11 nM) was incubated with 10^{-6}-10^{-3} M NaF and 175 µM PP_i for 10 min at 30 °C in a buffer containing 1 mM Mg^{2+} (●). Apyrase (68 nM) was incubated with 10^{-6}-10^{-3} M $GdCl_3$ and 250 µM GTP for 2.5 hours at 30 °C in a buffer containing 5 mM Ca^{2+} (○) before being diluted in a 2 mM Zn^{2+} containing buffer and exposed to JR2EC-AuNPs.

As the transduction mechanism is completely decoupled from the recognition event the enzymatic hydrolysis of PP_i to P_i by pyrophosphatase (PPase) could also be monitored using the same strategy. The hydrolysis of PP_i only yields two P_i as compared to three P_i for degradation of ATP by ALP (Figure 2a). Consequently, a higher initial concentration of PP_i was required than for the corresponding hydrolyzation of ATP by ALP to ensure that the AuNPs remained dispersed after complete hydrolysis of the substrate. The initial concentration of PP_i was set to 175 µM and was incubated with 0-11.3 nM PPase in a Tris buffer (50 mM, pH 7.2) containing 1 mM Mg^{2+} at 30 °C, which are the optimal conditions for PPase, for 10 min prior to addition of Zn^{2+} and JR2EC-AuNPs (Figure 2c). No effect on the normal mode of aggregation was observed in the absence of PPase (175 µM PP_i and 2 mM Zn^{2+}) or in the absence of PP_i (2 mM Zn^{2+} and 56 nM PPase) (Figure S4). A response was only obtained when both PP_i and PPase were present and the magnitude of the resulting LSPR shift was similar to that of ALP confirming that the nanoparticle aggregation was specific and the result of hydrolyzation of PP_i by PPase. The enzymatic degradation of PP_i (175 µM) by PPase (1.1-11.3 nM) was monitored as a function of time and PPase concentration (Figure 4b). Similarly to ALP, PPase displayed a linear correlation between $t_{½}$ and log[PPase] with a slope of the curve reflecting the catalytic activity for hydrolysis of the substrate used (Figure 4c).

The flexibility of this system also enabled characterization of enzyme substrate specificity. This was demonstrated using the phosphatase apyrase that catalyzes the hydrolysis of pyrophosphate bonds from various nucleoside di- and triphosphates with the sequential release of two equivalents of P_i (Figure 2a).[32] ATP and GTP were used as substrates and the initial concentrations were set to 250 µM to ensure a sufficient P_i generation to obtain fully dispersed particles after complete substrate hydrolysis within a reasonable timeframe since apyrase has a turnover rate which is only about a third of that of ALP.[33, 34] The concentration of apyrase was varied from 0 to 68 nM and the samples were incubated in a Mes buffer (50 mM, pH 6) containing 5 mM Ca^{2+} and 250 µM ATP or GTP for 2.5 hours at 30°C prior to Zn^{2+} and JR2EC-AuNP exposure (Figure 2d). The LSPR peak positions were fitted to a monophasic Hill equation yielding two separated functions representing the substrate preference for ATP over GTP (Figure 5a). The concentration of apyrase required to obtain a 50% response for ATP and GTP were found to be 12.7 and 17.9 nM, respectively, giving a substrate preference for ATP by a factor 1.41. Control experiments performed in the absence of apyrase (250 µM ATP or GTP and 2 mM Zn^{2+}) or in the absence of ATP or GTP (68 nM apyrase and 2 mM Zn^{2+}) did not affect the normal mode of aggregation, clearly demonstrating that the LSPR response was caused by apyrase hydrolyzation of ATP or GTP and indeed specific (Figure S5). The cofactor Ca^{2+}, present at a

concentration of 250 μM, is essential for apyrase activity. Ca^{2+} interacts less strongly with the nucleotides and the generated products as compared to Zn^{2+} (Table 1),[26, 30] but forms complexes with P_i to the same extent as Zn^{2+}.[29] A slightly higher P_i generation was consequently required in order to compensate for this interaction. The direct influence of Ca^{2+} on the aggregation of the polypeptide modified nanoparticles was negligible since Ca^{2+} does not induce folding of the polypeptides.[21]

Inhibitor characterization

We then went on to investigate the applicability of the assay for inhibition studies of the selected phosphatases. At least one inhibitor was used for each phosphatase and the concentration dependent response was characterized. Control experiments for all inhibitors were performed by monitoring the effects on aggregation of individual inhibitors present at the highest concentration used in the enzyme inhibition studies, with and without 2 mM Zn^{2+} (Figure S6). No inhibitor was found to influence the normal mode of aggregation or induce nanoparticle aggregation on their own. For ALP two distinctly different inhibitors were used: theophylline which is a methylxanthine drug used in therapy for respiratory disorders that inhibits ALP in an uncompetitive manner and sodium orthovanadate (Na_3VO_4) which is a transition state analog of P_i and acts as a competitive inhibitor.[35, 36] Both inhibitors (10^{-6}-10^{-3} M) showed dose responsive curves when incubated with 20 nM ALP and 100 μM ATP at 37 °C for 30 min (Figure 5b). An IC_{50} value of 102 μM was obtained for theophylline by fitting the data to a monophasic Hill equation, which is identical to previously reported data.[36] The IC_{50} value of Na_3VO_4 was 202 μM, which is slightly higher than previously reported values for alkaline phosphatases.[35] The dose responsive inhibition of PPase by sodium fluoride (NaF, 10^{-6}-10^{-3} M) and that of apyrase by gadolinium chloride ($GdCl_3$, 10^{-6}-10^{-3} M) gave IC_{50} values of 6.4 μM and 47 μM (Figure 5b), respectively, which are in good agreement with previously reported data.[24, 37]

Experimental

Materials: Alkaline phosphatase from bovine intestinal mucosa *(EC 3.1.3.1)*, apyrase from *Solanum tuberosum (EC 3.6.1.5)*, pyrophosphatase from *Saccharomyces cerevisiae (EC 3.6.1.1)*, inhibitors, metal salts (MCl_x), buffers and phosphate containing compounds were purchased from Sigma Aldrich and used without further purification. Citrate stabilized AuNPs with an average size of 20 nm was purchased from BBInternational.

Peptide synthesis: The polypeptide JR2EC (H_2N-AADLEK AIEALEKHLEAKGPCDAAQLEKQLEQAFEAFERAG-COOH) was synthesized on a Quartet automated peptide synthesizer (Protein Technologies, Inc.) using standard fluroenylmethoxycarbonyl (Fmoc) chemistry. The synthesis was performed on a 0.1 mmol scale with Fmoc-Gly-Wang (Iris biotech GMBH) with a substitution level of 0.77 $mmolg^{-1}$ as solid support. Each coupling was performed using a fourfold excess of O-(7-benzotriazole-1-yl)-1, 1, 3, 3-tetramethyluronium tetrafluoroborate, (TBTU, Iris biotech GMBH) as activator and an eightfold excess of diisopropylamine (DIPEA, Iris biotech GMBH) as base. A fourfold excess of amino acid (Iris biotech GMBH) was used in each coupling and subsequent deprotection of the coupled amino acid was accomplished by treatment with piperidine in DMF (20%, Applied Biosystems). Side chain deprotection and cleavage from the solid support was accomplished by exposure to a solution containing trifluoroacetic acid (TFA), ethandithiol, water and triisopropylsilane (TIS) (94:2.5:2.5:1, v/v/v/v) 15 mLg^{-1} of polymer for 2 hours followed by filtration and evaporation of the solvent. The crude peptide was precipitated twice in cold diethylether and then lyophilized. Purification of the crude peptide was carried out using a 30 minute gradient of 30-41 % aqueous isopropanol with 0.1 % TFA on an ACE 5 C-8 column (250 x 21.2 mm) attached to a semi-preparative HPLC system (Dionex). The identity of the purified peptide was confirmed by MALDI-TOF MS using an α–cyano-4-hydroxycinnamic acid matrix.

Gold nanoparticle functionalization: JR2EC functionalized AuNPs were acquired by incubating 10 μM JR2EC (10 mM sodium citrate, pH 6) with ~70 nM AuNPs for at least 18 hours at 4°C. The AuNPs were then repeatedly centrifuged and the supernatant was exchanged for Bis-Tris buffer (30 mM, pH 7.0), this procedure was repeated until the concentration of non-immobilized JR2EC was below 5 pM. The final concentration of the functionalized AuNPs was estimated to be approximately 6.8 nM using the absorbance at 526 nm and an extinction coefficient of 1.57 x 10^9 M^{-1} cm^{-1}.[38]

Colorimetric detection of phosphatase activity and inhibition: A colorimetric assay for enzymatic dephosphorylation / inhibition was performed as follows:

Alkaline phosphatase (ALP): ATP (5 μl, 20 mM, in MQ-water) and 10 μl ALP (0.01-50 μM, in 50 mM Tris buffer, pH 9) was added to a Tris buffer (50 mM, pH 9) containing 1 mM $MgCl_2$ giving a final volume of 50 μl. The samples were incubated in a water bath for 0 – 250 min at 37 °C. In the case of an inhibition experiment 5 μl of the inhibitor (10^{-5}-10^{-2} M) was added to the reaction mixture pre-incubation and then incubated for 30 min at 37 °C.

Pyrophosphatase (PPase): Pyrophosphate (8.75 μl, 20 mM, in MQ-water) and 10 μl PPase (5.5-280 nM, in 50 mM Tris buffer, pH 7.2) was added to a Tris buffer (50 mM, pH 7.2) containing 1 mM $MgCl_2$ giving a final volume of 50 μl. The samples were incubated in a water bath for 0 – 100 min at 30 °C. In the case of an inhibition experiment 5 μl of the inhibitor (10^{-5}-10^{-2} M) was added to the reaction mixture pre-incubation and then incubated for 10 min at 30 °C.

Apyrase: GTP (12.5 μl , 20 mM, in MQ-water) and 10 μl apyrase (17-340 nM, in 50 mM Mes buffer, pH 6) was added to a Mes buffer (50 mM, pH 6) containing 5 mM CaCl2 giving a final volume of 50 μl. The samples were incubated in a water bath for 0 – 180 min at 30 °C. In the case of an inhibition experiment 5 μl of the inhibitor (10^{-5}-10^{-2} M) was added to the reaction mixture pre-incubation and then incubated for 180 min at 30 °C.

COLORIMETRIC DETECTION: The sample (50 µl) incubated as above was added to 740 µl of Bis-Tris buffer (30 mM, pH 7) followed by addition of 10 µl JR2EC-AuNPs (6.8 nM). Bis-Tris buffer (200 µl, 30 mM, pH 7) containing 10 mM $ZnCl_2$ was added and the sample was incubated at room temperature for 20 min before UV-vis measurements.

CHARACTERIZATION: UV-vis measurements were performed in room temperature on a SHIMADZU UV-2450 spectrophotometer with a 0.5 nm resolution. TEM images were acquired using a Tecnai G2 F20U-Twin microscope operating at 200kV. Carbon coated TEM grids were prepared by applying 15 µL of sample and incubating for 30 min before removal of excess sample using filter paper.

Conclusions

We have developed a generic and flexible colorimetric AuNP-based strategy for monitoring the enzymatic hydrolysis of PP_x (ATP, ADP, AMP, GTP and PP_i) by phosphatases where the substrate recognition is completely decoupled from the nanoparticle stability modulation mechanism. This strategy enables detection of a wide range of enzymes using different natural, non-modified, substrates with a single detection system. The enzymatic reactions were transduced into a readily detectable optical signal using gold nanoparticles functionalized with a Zn^{2+}-responsive polypeptide. The nanoparticles aggregated when exposed to Zn^{2+} in the concentration range 1.5 – 2 mM, caused by a polypeptide folding-induced bridging that was triggered by the coordination of Zn^{2+} by the peptide. PPx and Pi also coordinate Zn^{2+}, and their presence interfered with the polypeptide folding and thus the nanoparticle aggregation. The various phosphatase substrates (PP_x) and the enzymatically generated byproduct phosphate (P_i) showed significant differences in coordination capacity for Zn^{2+}. Using this Zn^{2+}-responsive polypeptide-nanoparticle hybrid system the enzymatic hydrolyzation of PP_x could be monitored in real time by exploiting the large shifts in the localized surface plasmon resonance band as an indicator of enzymatic activity. The flexibility of this sensing strategy was evaluated using three completely different phosphatases; alkaline phosphatase, pyrophosphatase and apyrase that catalyze the enzymatic degradation of ATP, PP_i and GTP/ATP, respectively. All three enzymes could be detected in the low nanomolar range. Importantly, no interference from different metal cation cofactors was observed because of the preference of the polypeptide for coordinating Zn^{2+}. We also investigated the possibility to use this detection strategy for characterization of both enzyme substrate specificity and effects of inhibitors on enzymatic activity using different enzymes and substrates. The flexibility and versatility of this strategy clearly demonstrate the benefit of decoupling the biomolecular recognition event and the mechanism for nanoparticle stability modulation. The general applicability of this approach for detection of phosphatase activity, and for characterization of substrate specificity and phosphatase inhibitors is expected to be of significant value for the development of novel diagnostic assays and high-throughput drug screening.

Acknowledgements

The authors acknowledge the financial support from Linköping University, the Swedish Research Council (VR), the Swedish Foundation for Strategic Research (SSF), the Knut and Alice Wallenberg Foundation (KAW) and the Centre in Nanoscience and Technology (CeNano). We thank Erik Martinsson for help with graphics. During this study R.S. was enrolled in the graduate school Forum Scientium.

Notes and references

Division of Molecular Physics, Department of Physics, Chemistry and Biology, Linköping University, SE-583 36 Linköping, Sweden
E-mail: daniel.aili@liu.se
Electronic Supplementary Information (ESI) available: See DOI: 10.1039/b000000x/

1. G. Burnstock, *Trends Pharmacol. Sci.*, 2006, **27**, 166.
2. H. A. Praetorius and J. Leipziger, *Annu. Rev. Physiol.*, 2010, **72**, 377.
3. C. A. Parent and P. N. Devreotes, *Science*, 1999, **284**, 765.
4. E. Cabib, J. Drgonová and T. Drgon, *Annu. Rev. Biochem.*, 1998, **67**, 307.
5. W. E. Balch, *Trends Biochem. Sci.*, 1990, **15**, 473.
6. R. A. Terkeltaub, *Am. J. Physiol.-Cell PH.*, 2001, **281**, C1.
7. A. R. Saltiel and C. R. Kahn, *Nature*, 2001, **414**, 799.
8. B. Boivin, F. Chaudhary, B. C. Dickinson, A. Haque, S. C. Pero, C. J. Chang and N. K. Tonks, *J. Biol. Chem.*, 2013, **288**, 36926.
9. S. Klumpp and J. Krieglstein, *Curr. Opin. Pharmacol.*, 2002, **2**, 458.
10. R. Q. Thompson, G. C. Barone Iii, H. B. Halsall and W. R. Heineman, *Anal. Biochem.*, 1991, **192**, 90.
11. J. S. Blum, R. H. Li, A. G. Mikos and M. A. Barry, *J. Cell. Biochem.*, 2001, **80**, 532.
12. L. Jia, J.-P. Xu, D. Li, S.-P. Pang, Y. Fang, Z.-G. Song and J. Ji, *Chem. Commun.*, 2010, **46**, 7166.
13. N. L. Rosi and C. A. Mirkin, *Chem. Rev.*, 2005, **105**, 1547.
14. D. Aili and M. M. Stevens, *Chem. Soc. Rev.*, 2010, **39**, 3358.
15. R. Wilson, *Chem. Soc. Rev.*, 2008, **37**, 2028.
16. D. Aili, M. Mager, D. Roche and M. M. Stevens, *Nano Lett.*, 2010, **11**, 1401.
17. D. Aili, R. Selegard, L. Baltzer, K. Enander and B. Liedberg, *Small*, 2009, **5**, 2445.
18. A. Laromaine, L. L. Koh, M. Murugesan, R. V. Ulijn and M. M. Stevens, *J. Am. Chem. Soc.*, 2007, **129**, 4156.
19. R. Elghanian, J. J. Storhoff, R. C. Mucic, R. L. Letsinger and C. A. Mirkin, *Science*, 1997, **277**, 1078.
20. J.-S. Lee, M. S. Han and C. A. Mirkin, *Angew. Chem., Int. Ed.*, 2007, **46**, 4093.
21. D. Aili, K. Enander, J. Rydberg, I. Nesterenko, F. Björefors, L. Baltzer and B. Liedberg, *J. Am. Chem. Soc.*, 2008, **130**, 5780.

22. C. M. Li, S. J. Zhen, J. Wang, Y. F. Li and C. Z. Huang, *Biosens. Bioelectron.*, 2013, **43**, 366.
23. W. Zhao, W. Chiuman, J. C. F. Lam, M. A. Brook and Y. Li, *Chem. Commun.*, 2007, 3729.
24. J. Deng, Q. Jiang, Y. Wang, L. Yang, P. Yu and L. Mao, *Anal. Chem.*, 2013, **85**, 9409.
25. H. L. Clever, M. E. Derrick and S. A. Johnson, *J. Phys. Chem. Ref. Data*, 1992, **21**, 941.
26. H. Sigel and R. Griesser, *Chem. Soc. Rev.*, 2005, **34**, 875.
27. H. Sigel, E. M. Bianchi, N. A. Corfù, Y. Kinjo, R. Tribolet and R. B. Martin, *Chem.-Eur. J.*, 2001, **7**, 3729.
28. M. Mak, R. Selegård, M. Garbrecht and D. Aili, *Part. Part. Syst. Charact*, 2014, In press.
29. F. X. Han, *Biogeochemistry of trace Elements in Arid Environments*, Springer, Dordrecht, 2007.
30. E. M. Bianchi, S. A. A. Sajadi, B. Song and H. Sigel, *Chem.-Eur. J.*, 2003, **9**, 881.
31. H. A. Azab and Z. M. Anwar, *J. Chem. Eng. Data*, 2012, **57**, 2890.
32. L. Plesner, in *International Review of Cytology*, eds. W. J. Kwang and J. Jonathan, Academic Press, 1995, vol. Volume 158, pp. 141.
33. A. M. Kettlun, V. Espinosa, L. García and M. A. Valenzuela, *Phytochemistry*, 2005, **66**, 975.
34. T. Manes, M. F. Hoylaerts, R. Müller, F. Lottspeich, W. Hölke and J. L. Millán, *J. Biol. Chem.*, 1998, **273**, 23353.
35. P. J. Stankiewicz and M. J. Gresser, *Biochemistry*, 1988, **27**, 206.
36. E. N. Fawaz and A. Tejirian, *Hoppe Seylers Z. Physiol. Chem.*, 1972, **353**, 1779.
37. A. Escalada, P. Navarro, E. Ros, J. Aleu, C. Solsona and M. Martín-Satué, *Neurochem. Res.*, 2004, **29**, 1711.
38. J. Yguerabide and E. E. Yguerabide, *Anal. Biochem.*, 1998, **262**, 137.